

# Remodeling of the Extracellular Matrix by Endothelial Cell-Targeting siRNA Improves the EPR-Based Delivery of 100 nm Particles

Yu Sakurai<sup>1</sup>, Tomoya Hada<sup>1</sup>, Shoshiro Yamamoto<sup>1</sup>, Akari Kato<sup>1</sup>, Wataru Mizumura<sup>1</sup> and Hideyoshi Harashima<sup>1</sup>

<sup>1</sup>Faculty of Pharmaceutical Sciences, Hokkaido University, Kita-ku, Sapporo, Japan.

A number of nano drug delivery systems have recently been developed for cancer treatment, most of which are based on the enhanced permeability and retention effect. The advantages of the enhanced permeability and retention effect can be attributed to immature vasculature. Herein we evaluated the intratumoral distribution of lipid nanoparticles when the VEGF receptor 2 on tumor endothelial cells was inhibited by liposomal siRNA. VEGF receptor 2 inhibition resulted in an increase in intratumoral distribution and therapeutic efficacy despite the maturation of the tumor vasculature. A small molecule inhibitor against matrix metalloproteinase and macrophage depletion cancelled the improvement in the distribution of the lipid nanoparticles, suggesting that remodeling of tumor microenvironment played a role in the facilitated intratumoral distribution via the down-regulation of VEGF receptor 2. Accordingly, our results suggest that the enhanced permeability and retention effect is dependent, not only on the structure of the tumor vasculature, but also on the dynamics of the tumor microenvironment including extracellular matrix remodeling. Regulating the tumor microenvironment and the extracellular matrix by delivering tumor endothelial cell-targeting siRNA could potentiate the enhanced permeability and retention effect-based strategy.

Received 27 June 2016; accepted 7 September 2016; advance online publication 15 November 2016. doi:10.1038/mt.2016.178

## INTRODUCTION

Over the past decades, a number of groups have reported on the development of tumor-targeting nanoparticles, most of which function based on the enhanced permeability and retention (EPR) effect.<sup>1</sup> The EPR effect involves the systemic injection of macromolecules with a long circulation time that can passively accumulate in tumor tissue because the high levels of vascular endothelial growth factor (VEGF) in tumor tissue makes the vasculature porous and leaky.<sup>2</sup> On the other hand, recent studies revealed that components of the extracellular matrices (ECMs), such as collagen and hyaluronan, are major obstacles to the intratumoral diffusion

of cancer-targeted nanoparticles.<sup>3</sup> The high density of cells, in addition to abundant ECMs in tumor tissue, results in an elevated interstitial fluid pressure (IFP), which is inverse from the extracellular space to the capillary.<sup>4</sup> Additionally, these ECMs sterically hinder the diffusion of nanoparticles. In fact, it has been shown that the enzymatic degradation of these components by collagenase or hyaluronidase treatment resulted in the improved delivery of nano-sized therapeutics.<sup>5,6</sup> The effect of ECMs would be predicted to be proportional to the size of nanoparticles. Cabral *et al.*, recently confirmed this, by showing that small-sized nanoparticles with a diameter of 30 nm penetrated more deeply into tumor tissue than large-sized nanoparticles with a diameters of 100 nm in a hypovascular cancer model.<sup>7</sup> These collective findings indicate that ECMs severely restrict the intratumoral distribution of 100 nm nanoparticles. Accordingly, regulating tumor microenvironment including abnormal vasculature and ECMs should be required for further development of cancer-targeted nano medicines. Nowadays, a much attention has been paid for controlling tumor microenvironment for a more efficient cancer targeting.<sup>8,9</sup>

Recently, we accidentally discovered that an inhibition of VEGF signaling in the tumor endothelial cells (TECs) by siRNA unexpectedly elevated an accumulation and an intratumoral distribution of nanoparticles in human renal cell carcinomas (RCCs), which is known to be a highly vascularized cancer.<sup>10</sup> This improvement must be unexplainable through the basis of EPR effect that the malformed vasculature is responsible for EPR-based delivery. In this manuscript, we tried to elucidate the mechanism on this unknown increase in the accumulation and intratumoral distribution of nanoparticles. Our hypothesis is as follows; (i) VEGF signaling abnormally overexpressed in TECs, is inhibited by siRNA; (ii) TECs regulated by siRNA attracts some cell population; (iii) The attracted cell population degrades ECMs by some proteases; and (iv) This series of phenomenon after the inhibition in VEGF signaling alters tumor microenvironment for an appropriate distribution of nanoparticles.

To prove our hypothesis, we examined the effect of VEGF receptor 2 (VEGFR2) inhibition on the intratumoral distribution of lipid nanoparticles (LNPs) and the dynamics of ECMs in highly vascularized cancer RCCs. For the *in situ* down-regulation of a specific gene on TECs, we used a cyclic RGD-modified liposomal

The first two authors contributed equally to this work.

Correspondence: Hideyoshi Harashima, Faculty of Pharmaceutical Sciences, Hokkaido University, Kita-12, Nishi-6, Kita-ku, Sapporo 060-0812, Japan.  
E-mail: harasima@pharm.hokudai.ac.jp

siRNA (RGD-MEND). This is because delivering a siRNA specifically to TECs circumvents off-target effects in other cells such as cancer cells and stromal cells, indicating that a small molecule or an antibody can affect the function of other cell populations. In addition, the RGD-MEND had no effect on endothelial cells in normal organs.<sup>11</sup> Therefore, we were able to analyze the effect of gene silencing exclusively in TECs. The lipid envelope of the RGD-MEND was composed of YSK05, a pH-sensitive cationic lipid. The acid dissociation constant,  $pK_a$ , of YSK05 is ~6.5, which allows YSK05-containing liposomes to be biocompatible in the blood stream, where the pH is maintained at 7.4. In addition, the positive charge under acidic conditions resulted in efficient membrane fusion after the internalization of the particles by cells. This explains why YSK05-containing MENDs are able to deliver siRNA and suppress a gene of interest in hepatocytes, tumor tissue.<sup>12,13</sup> In this study, cyclic RGD, which recognizes the  $\alpha_v\beta_3$  integrin heterodimer, was used as a specific ligand for TECs that express high levels of  $\alpha_v\beta_3$  integrin.<sup>14</sup> Owing to these functional devices, the RGD-MEND had the ability to inhibit a TEC gene at a dose of 0.75 mg siRNA/kg.<sup>11,15</sup>

We investigated the alteration in the intratumoral distribution of nano drug delivery systems (DDSs) and the tumor microenvironment after vasculature maturation via the inhibition of VEGFR2 on TECs by the RGD-MEND. Our results suggest that vasculature leakiness as the result of immature vessels is not necessarily required for the extravasation of LNPs, at least in hypervascular cancer, and that carefully controlling the tumor microenvironment, including ECMs, has the potential for maximizing the therapeutic effect of nanoparticles.

## RESULTS

### VEGFR2 knockdown and consequent changes of intratumoral distribution

We first examined the silencing efficacy of RGD-MEND encapsulating siRNA against murine VEGFR2 (si-VR2) with human RCC, OS-RC-2-bearing mice. RCCs are characterized as a highly vascularized form of cancer, mainly due to the excessive amount of VEGF that is produced, due to the von Hippel Lindau factor is absent.<sup>16</sup> The LNPs used contained the pH-sensitive lipid, YSK05, and details of their characterization are shown in **Supplementary Figure S1**). Injection of the RGD-MEND significantly inhibited VEGFR2 expression in terms of both the mRNA and protein level (**Supplementary Figure S2a–c**). A single injection of the RGD-MEND partially succeeded in improving penetration of the LNPs, but that was observed only in a small area of the tumor tissue by confocal laser scanning microscopy (see **Supplementary Figure S3**). We speculated that a level of VEGFR2 knockdown is not sufficient and too short to alter the tumor microenvironment. This is because VEGFR2 dissipated rapidly because the TECs grew more rapidly than normal cells.<sup>17</sup> In nonproliferative tissues, such as the liver, gene silencing is observed, at least, for a week.<sup>18</sup> The concentration of siRNA would be diluted by the rapid proliferation. Therefore, we administered si-VR2 encapsulated in the RGD-MEND continuously over a period of 4 days. Confocal laser scanning microscopy revealed that the distribution of the LNPs was obviously altered and the distribution was increased by 1.9-fold as the result of a pretreatment with the RGD-MEND

(**Figure 1b,c**). Further, the improvement in intratumoral distribution was reproducible despite the short-lived knockdown of VEGFR2 (see **Supplementary Figure S2a**). The improvement appeared to be achieved when the concentration of VEGFR2 was sufficiently decreased for a certain time. To quantitatively measure the intratumoral distribution, single cancer cells from tumor tissues were subjected to fluorescence-activated cell sorting (FACS, **Supplementary Figure S4**). The fluorescence intensity of the LNPs were increased by 2.1-fold and the coefficient of variance (CV) was decreased (**Figure 1d,e**). In addition, not only the distribution but also level of accumulation was significantly augmented (**Figure 1f**). On the other hand, particle accumulation in normal organs was not changed except for the spleen (see **Supplementary Figure S5**). In addition, when a control siRNA was assembled in the RGD-MEND, the intratumoral distribution of LNPs was not altered (see **Supplementary Figure S6**). It is possible that the increased accumulation of LNPs (**Figure 1f**) could be attributed to the widened intratumoral distribution of LNPs. However, a 2.67-fold increase in the amount of systemically administered LNPs failed to result in the broad intratumoral distribution of LNPs (see **Supplementary Figure S7**). Therefore, another factor aside from the elevated accumulation of LNP appears to be responsible for the increased intratumoral accumulation.

To assess the impact of improving the intratumoral distribution of LNPs on therapeutic efficacy, OS-RC-2-bearing mice were administered doxorubicin-loaded liposomes (DOX-LNP, characterized in **Supplementary Figure S1**) and an RGD-MEND encapsulating si-VR2 at the same time. As a result, only the coinjection resulted in a substantial inhibition of tumor growth (**Figure 1g**). Incidentally, only the injection of the RGD-MEND led to a moderate inhibition of tumor growth. This suppression was interpreted as being due to the antiangiogenic effect of VEGFR2 inhibition via the delivery of siRNA to TECs. We previously confirmed that an RGD-MEND encapsulating si-VR2 caused a delay in tumor growth by decreasing the density of microvessels in tumor tissue.<sup>15</sup> On the other hand, a continuous treatment (3 separate injections of the RGD-MEND was started prior to the first injection of DOX-LNP) and the results indicated a more moderate therapeutic effect (not data shown). This can be attributed to short-lived silencing by the RGD-MEND (< 72 hours). These results suggest that si-VR2 induced an alteration in the tumor microenvironment as well as increasing the accumulation of LNPs in tumors. In summary, the broad distribution of LNPs resulting from VEGFR2 inhibition could result in a better therapeutic effect.

### Maturation of the tumor vasculature by liposomal siRNA against VEGFR2

We then explored the issue of whether the vasculature matured as the result of the continuous inhibition of VEGFR2 by the si-VR2-loaded RGD-MEND. Pericyte coverage is regarded as a marker of vessel maturation.<sup>19</sup> Injection of the RGD-MEND encapsulating si-VR2 significantly induced pericyte coverage around TECs (**Figure 2a,b**), and this increase was dependent of the dosage of siRNA used (**Figure 2c**). We then explored the functionality of the tumor vasculature. Since the immaturation of the tumor vasculature has known to be a cause of hypoxia because of diminished blood flow, staining with a hypoxia marker

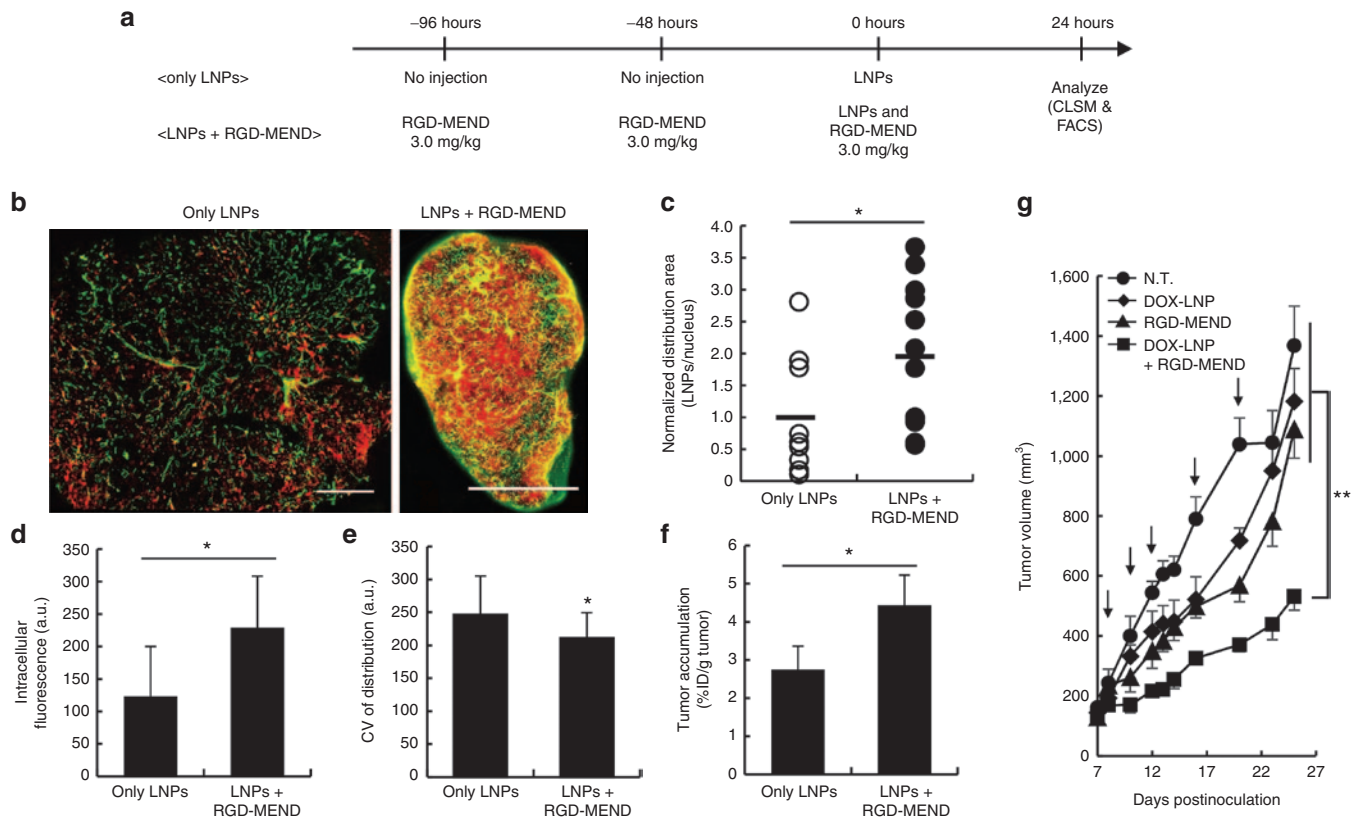


**Figure 1** Improvement in the subsequent distribution of LNPs' and efficacy after the continuous inhibition of VEGFR2. **(a)** Schematic diagram of experimental protocol. **(b)** Whole images of the intratumoral distribution of fluorescently labeled LNPs. Left panel and right panel denote only LNPs and LNPs with pretreatment of three RGD-MEND injections, respectively. Red dots and green dots denote LNPs and tumor endothelium, respectively. Scale bars: 1,000  $\mu\text{m}$ . **(c)** Areas of red pixels were calculated with ImageJ software. Pixel area of the LNPs were normalized by nucleus areas ( $n = 9-11$ ). **(d)** Fluorescent intensity and **(e)** coefficient of variance of histogram of single dispersed cancer cells were determined by FACS analysis. **(f)** Accumulation of LNPs was determined using radioisotope labeled-LNPs. Radioactivity of LNPs labeled with [<sup>3</sup>H]-cholesteryl hexadecyl ether was measured by liquid scintillation counting at 24 hours after the injection. **(g)** The effect of improved intratumoral distribution on anticancer treatment by liposomal-doxorubicin (DOX-LNP). After the tumor volume reached 100 mm<sup>3</sup>, DOX-LNP and/or the RGD-MEND were administered five times ( $n = 5$ ). Tumor volumes were chronologically measured according to the equation = (major axis (mm))  $\times$  (minor axis (mm))<sup>2</sup> / 2. Arrows indicate the injection of therapeutics. LNPs, lipid nanoparticles; FACS, fluorescence-activated cell sorting; RGD-MEND, RGD-modified liposomal siRNA; VEGFR2, VEGF receptor 2.

pimondazole was performed. Hypoxic regions were significantly suppressed in the RGD-MEND-treatment group (Figure 2d,e). Moreover, the functional vasculature was visualized by comparing the vasculature stained by the systemic injection of fluorescein isothiocyanate (FITC)-isolectin B4 and the positive vasculature by immersion in alexa647-isolectin B4 positive vasculature after sacrifice. The RGD-MEND treatment resulted in an increase in vasculature stained by both isolectins, suggesting that the blood flow was recovered as the result of injecting the RGD-MEND (Figure 2f,g). These results show that delivering siRNA by the RGD-MEND led to vascular maturation in terms of both structure and function, and implies that the maturation of the tumor vasculature did not necessarily inhibit the extravasation and distribution of large nanoparticles (100 nm).

### Involvement of ECM remodeling on an altered tumor microenvironment for delivering nanoparticles

ECMs are one of the possible factors that restrict the tumor penetration of LNPs due to steric hindrance and an increase in IFP. Next, we focused on Type 1 collagen, a major component of ECMs.

Type 1 collagen  $\alpha 1$  (COL1A1), which consists of Type 1 collagen chains, was found to be localized in the perivascular region and was distributed throughout the tumor sections (Figure 3a, left panels). On the other hand, the inhibition of VEGFR2 by the RGD-MEND significantly suppressed the expression of COL1A1 (Figure 3a, right panels and Supplementary Figure S8), and this decrease was dependent on the dosage of si-VR2 (Figure 3b). On the other hand, type IV collagen, a scaffold protein of the vasculature and regarded as a maturation marker, was increased slightly by the RGD-MEND, but the difference was not statistically significant (see Supplementary Figure S9). In addition, hydroxyproline, an amino acid that is specifically found in collagen and elastin,<sup>20</sup> was also decreased (Figure 3c). We inferred that the inhibition of VEGFR2 by the RGD-MEND resulted in the production of matrix metalloproteinases (MMPs), which are a series of enzymes that require a divalent metal ion for their activity and which catalyze the degradation of collagens and elastins,<sup>21</sup> thus leading to the degradation of collagen molecules. Actually, the mRNA levels of MMP-2 and -9 were drastically augmented by the RGD-MEND injection and this increase was dose-dependent (Figure 3d,e).

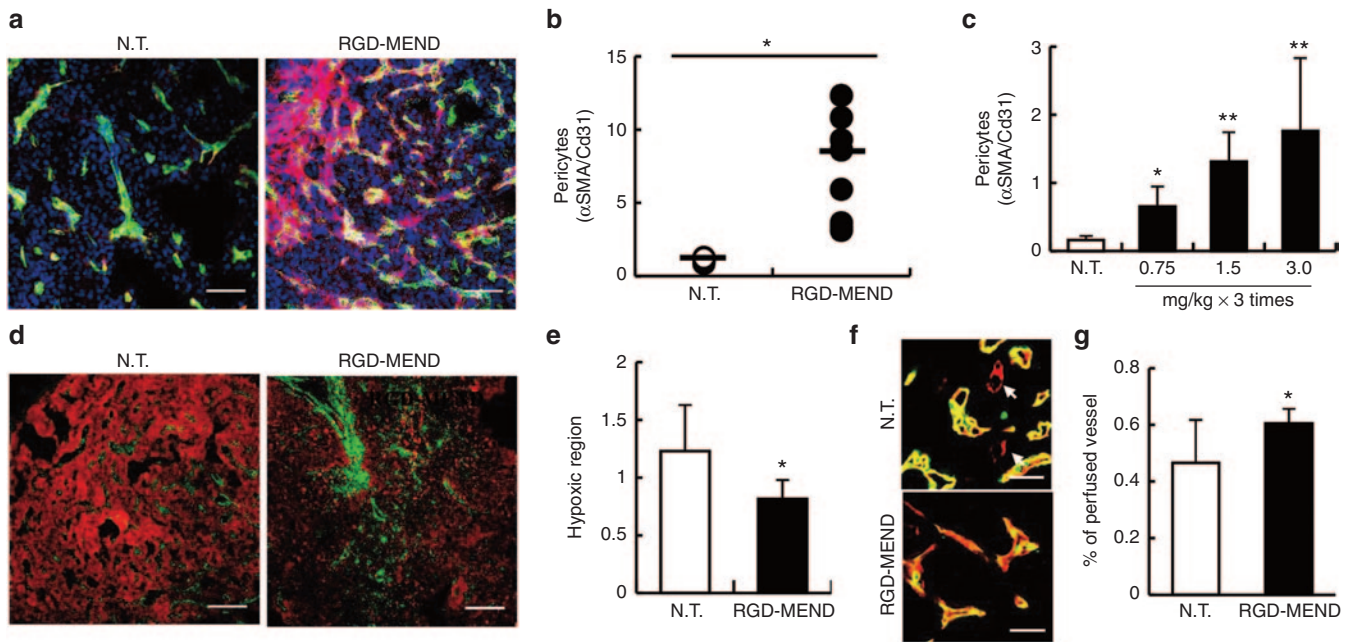


**Figure 2** Vascular maturation by siRNA against VEGFR2 encapsulated in the RGD-MEND. **(a)** Representative image of the increase in pericyte coverage by the RGD-MEND. Tumor tissues were cryo-sectioned after the continuous inhibition of VEGFR2. The sections were stained with Hoechst33342 (blue, nucleus), FITC-isolectin (green, vessels) and cy3- $\alpha$ SMA (red, pericytes). Scale bars: 100  $\mu$ m. **(b)** Quantitative data of **a**. Pixels were counted in nine images from three independent mice, and the red pixels (pericytes) were then normalized to green pixels (vessels). **(c)** Dose-dependency for the increase in pericyte coverage. Pericytes were counted when the dosages of si-VR2 varied from 0.75 mg/kg to 3.0 mg/kg (each groups were of three mice). **(d)** Decrease in hypoxic area in RGD-MEND-treated mice. Tumor tissues were collected 90 minutes after the injection of the hypoxia-probe pimonidazole. Green and red pixels vessels and the indicated hypoxic regions, respectively. Scale bars: 100  $\mu$ m. **(e)** Red dots indicating hypoxic regions were counted and normalized to nucleus areas. Data were obtained from nine images from three independent mice. **(f)** Recovery of blood flow by the RGD-MEND. FITC-isolectin B4 was systemically injected before sacrifice, and the collected tumor tissues were then immersed in Alexa647-isolectin B4. Arrows show the vasculature without blood flow. **(g)** Quantitative data of perfused vessels. Population of the vasculature with blood flows (shown as yellow) against all of the vasculature (shown as yellow and red) were counted. FITC, fluorescein isothiocyanate; RGD-MEND, RGD-modified liposomal siRNA; VEGFR2, VEGF receptor 2.

To verify that MMPs were involved in the distribution of LNPs and the degradation of COL1A1, we investigated a change in both of these components in presence of marimastat, a MMPs inhibitor. When OS-RC-2 tumor-bearing mice were treated with five separate injections of 30 mg/kg of marimastat during the continuous inhibition, the intratumoral distribution of LNPs decreased significantly (**Figure 3f-h**) compared with only the RGD-MEND treatment group. At this time, COL1A1 diminished by the injection of the RGD-MEND was elevated by a marimastat treatment. Taken together, the RGD-MEND injection facilitated the production of MMPs, and the subsequently produced MMPs degraded excess ECMs, such as Type 1 collagen. This explains the rapid diffusion of LNPs into the altered tumor mass.

### Altering nanoparticle distribution by macrophages through ECM degradation

Later, we attempted to identify which cell population produced MMPs. In tumor tissues, macrophages are a major source of MMPs.<sup>22</sup> We hypothesized that si-VR2 encapsulated in the RGD-MEND induced the infiltration of macrophages. First, we confirmed whether macrophages were localized in the tumor tissues by confocal laser scanning microscopy. Actually, macrophage levels were significantly increased by the RGD-MEND administration (**Figure 4a,b**) and most were adjacent to the vasculature. The substantial infiltration of macrophages into tumor tissue might

have originated in the spleen. A previous report revealed that the origins of tumor-associated macrophages and neutrophils were the spleen.<sup>23</sup> The transition of macrophages from the spleen to the tumor would lead to a decrease in the level of macrophages in the spleen, and consequently might alter the accumulation of LNPs in the spleen (see **Supplementary Figure S5**). To investigate the impact of macrophage infiltration, macrophages were depleted by a liposomal clondronate (L-clondronate) treatment. When 1.4 mg of L-clondronate was injected into the tail vein of mice, macrophages were completely removed (see **Supplementary Figure S11**). LNPs and formulated si-VR2 were systemically administered to OS-RC-2 bearing mice with or without L-clondronate. LNPs were more broadly distributed in the presence of L-clondronate (**Figure 4c,d**). At this time, L-clondronate significantly increased the levels of COL1A1 (**Figure 4e,f**). Accordingly, macrophages infiltrating into tumor tissues by the injection for RGD-MEND produced MMPs, and ECMs were subsequently broken down. In such a tumor microenvironment, LNPs would be able to readily diffuse into the tumor mass.

### DISCUSSION

The EPR effect is attributed to abnormal tumor vasculature with leaky intercellular junctions and intracellular fenestrae owing to overexpressed VEGF (<30-fold) in tumor tissue.<sup>24,25</sup> In fact, inflammatory factors, such as bradykinin and nitric oxide, facilitated the

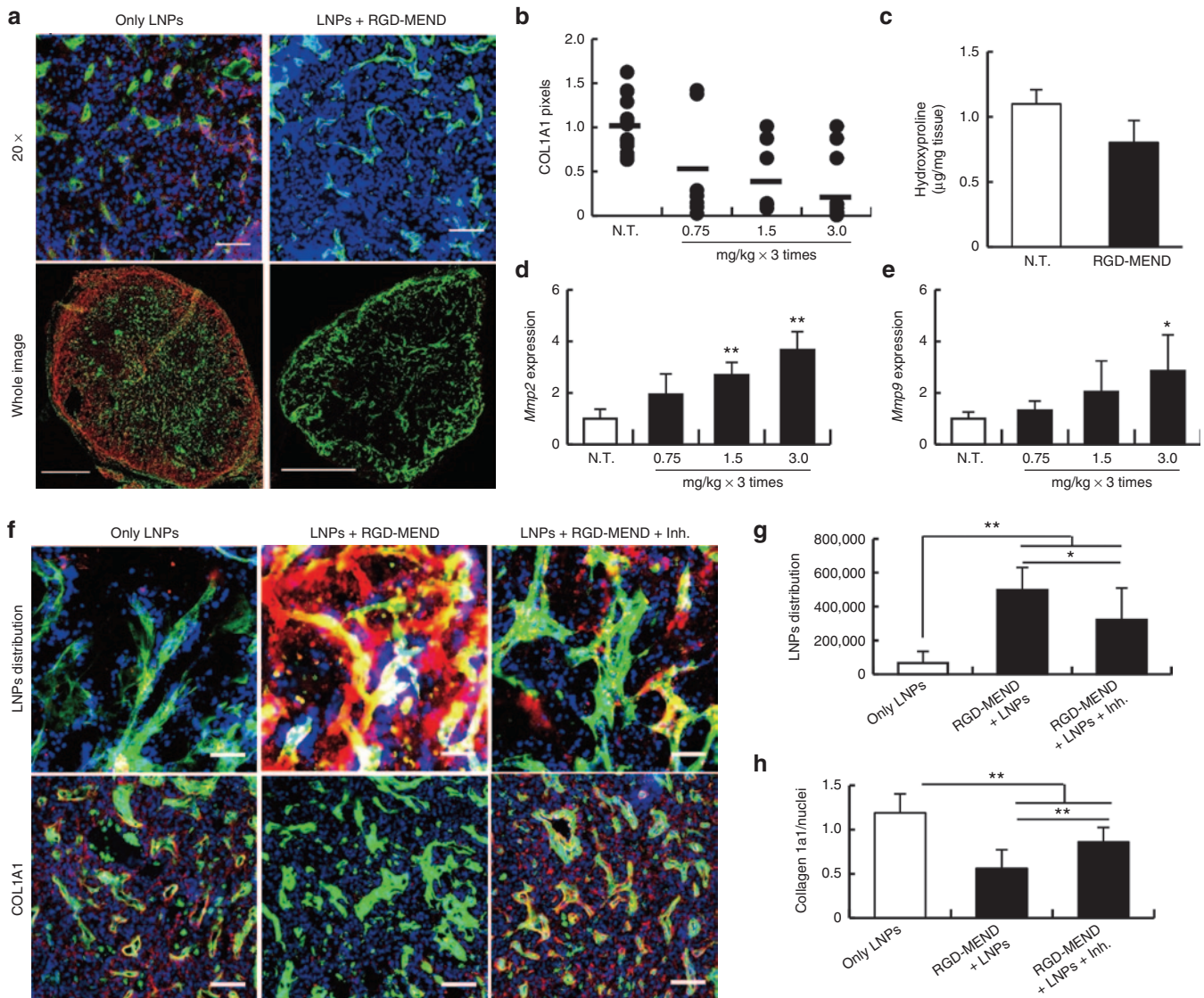


**Figure 3** Degradation of extracellular matrices (ECMs) by a matrix metalloproteinase induced via si-VR2 encapsulated in the RGD-MEND. **(a)** Degradation of collagen1a1 by the injection of RGD-MEND. Upper and lower panels represent magnified images of frozen sections (Scale bar: 50  $\mu$ m) and whole images (Scale bar: 1,000  $\mu$ m). Tumor sections after the RGD-MEND treatment were immunostained and observed by confocal laser scanning microscopy (CLSM). Green and red dots indicate vessels and COL1A1, respectively. **(b)** Red dots indicating COL1A1 were counted when si-VR2 dosages varied from 0.75 mg/kg to 3.0 mg/kg. **(c)** Decrease hydroxyproline levels in tumor tissue. The amount of hydroxyproline was determined by Ehrlich's reagent. **(d)** MMP-2 and **(e)** -9 expression level after the injection of the RGD-MEND. Expression level of MMPs 24 hours after three injections of the RGD-MEND was determined by quantitative RT-PCR. ANOVA was performed for statistical analysis, followed by SNK test. \* $P < 0.05$ . \*\* $P < 0.01$ . **(f)** The impact of MMP inhibitor Marimastat on LNP distribution and collagen degradation. In the upper panels, blue, green, and red dots indicate nuclei, vessels and LNPs, respectively (Scale bars: 100  $\mu$ m), observing raw sections. In the lower panels, red dots indicate COL1A1, and the others are the same as the upper panels (Scale bars: 100  $\mu$ m), observing frozen sections. **(g)** and **(h)** Pixel counts of LNPs and COL1A1. ANOVA was performed for statistical analysis, followed by SNK test. \*\* $P < 0.01$ . ANOVA, analysis of variance; LNPs, lipid nanoparticles; MMP, matrix metalloproteinases; RT-PCR, reverse-transcription polymerase chain reaction; RGD-MEND, RGD-modified liposomal siRNA.

extravasation of the pigment, Evans Blue.<sup>26</sup> In our study, VEGFR2 inhibition by siRNA significantly increased both tumor accumulation and the penetration of LNPs despite vasculature maturation (Figure 1b,f and Figure 2a–g), at least in hypervascular cancer human RCCs. The improvement in intratumoral distribution was caused by the remodeling of ECMs by infiltrating cells, not by the leakiness of the tumor vasculature. Figure 5 shows a summary of our study.

It is known that VEGFR2 is a major protein in primary angiogenesis in tumor tissue, and thus blocking the action of VEGFR2

would result in the inhibition of tumor growth via the antiangiogenic effect.<sup>27,28</sup> The relationship, however, between VEGFR2 and ECMs in the tumor tissue is not well validated. On the other hand, abundant ECMs are a typical symptom for fibrotic diseases in non-cancerous tissues, such as cirrhosis of the liver. In the case of normal organs, it was known that VEGFR2 plays a pivotal role in the progression of fibrosis, and the inhibition of VEGFR2 ameliorates fibrosis.<sup>29,30</sup> In addition, VEGFR2 inhibition was also reported to improve renal fibrosis in a fibrosis model<sup>31</sup> Although the exact mechanism responsible for the decomposition by blocking the

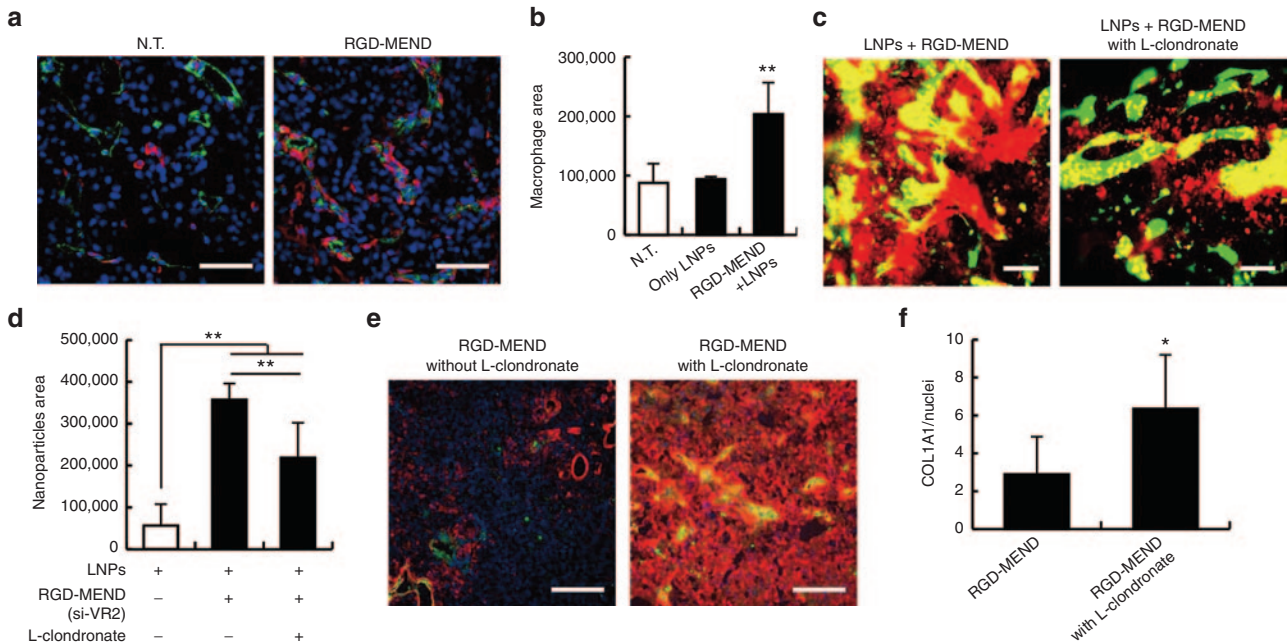


**Figure 4** Involvement of macrophages on the improvement in the intratumoral distribution of LNPs. **(a)** Increase in macrophages by si-VR2 encapsulated in the RGD-MEND. Blue, green and red dots indicate nuclei (Hoechst33342), vessel (FITC-isolectin) and macrophages (F4/80). Scale bars are 100  $\mu$ m. **(b)** Pixels indicating macrophages from **a** were counted by Image J. ANOVA was performed for statistical analysis, followed by the SNK test ( $n = 9-12$ ).  $**P < 0.01$ . **(c)** The effect of macrophage depletion on LNP distribution. Tumor sections were observed when liposomal clondronate (L-clondronate) was administered. Green and red dots indicate vessels and LNPs, respectively. Scale bars are 100  $\mu$ m. **(d)** Pixels indicating LNPs were counted, and analyzed by ANOVA, followed by SNK test ( $n = 9-12$ ).  $**P < 0.01$ . **(e)** COL1A1 change by the injection of L-clondronate. Blue, green and red dots showed nuclei, vessels and COL1A1, respectively. Scale bars are 50  $\mu$ m. **(f)** Pixels were quantified by Image J. Statistical analysis was performed by unpaired *t*-test.  $*P < 0.05$  ( $n = 9-12$ ). ANOVA, analysis of variance; FITC, fluorescein isothiocyanate; LNPs, lipid nanoparticles; RGD-MEND, RGD-modified liposomal siRNA.

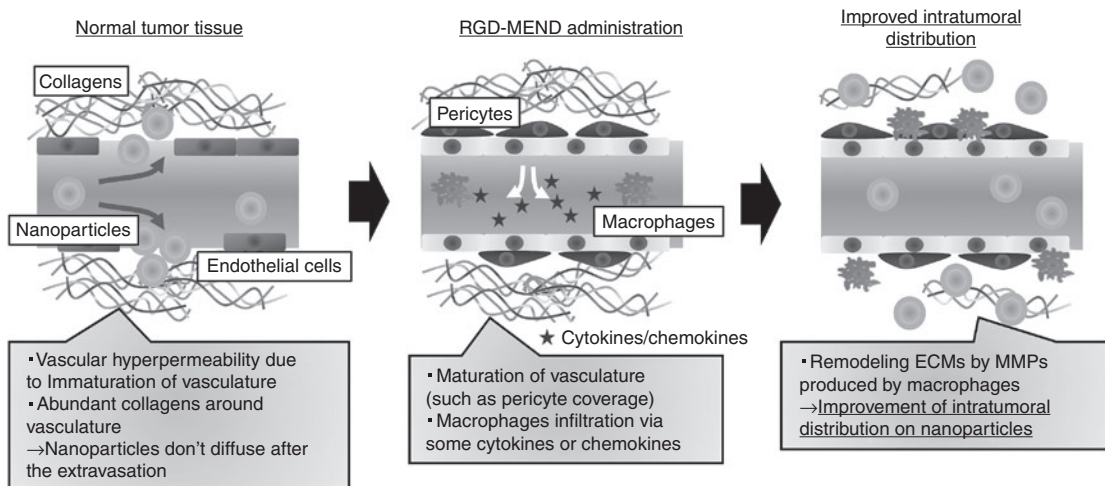


**Figure 5** Conceptual illustration of the improvement of intratumoral distribution of nanoparticles. In untreated tumor tissue, the tumor vasculature is immature. Specifically the vasculature lacks pericyte coverage and basement membrane and fenestrae (intracellular pore) and a loose junction (intercellular gap) exists. For these reasons, nanoparticles can pass through the vascular wall, a process that is called the EPR effect. However, the presence of abundant collagen molecules restrict the intratumoral diffusion of the nanoparticles. This study revealed that the inhibition of VEGFR2 on tumor endothelial cells (TECs) by the RGD-MEND leads to the infiltration of macrophages. The macrophages then produce matrix metalloproteinases (MMPs) that catalyze the degradation of the extracellular matrices (ECMs). After the remodeling of the ECMs, nanoparticles are able to penetrate more deeply into the tumor tissue. EPR, enhanced permeability and retention; RGD-MEND, RGD-modified liposomal siRNA; VEGFR2, VEGF receptor 2.

action of VEGFR2 is not understood, some reports have indicated that MMPs are involved.<sup>32</sup> Our hypothesis seems to be consistent with these results on the involvement between hepatic and renal fibrosis and VEGFR2.

Several studies have reported that reagents, such as bradykinin<sup>33</sup> and nitric oxide,<sup>25</sup> accelerate the development of hyper-vascularity in the tumor vasculature, thus improving EPR-based delivery. We initially expected that the blocking of VEGFR2 by

the RGD-MEND would improve the intratumoral distribution of LNPs, but not the accumulation of LNPs. However, the actual results indicated that the accumulation of LNPs was increased by 1.9-fold as the result of VEGFR2 inhibition, despite the maturation of the tumor vasculature. The mechanism responsible for how LNPs extravasate through mature vasculature is currently unclear. Tong RT *et al.*, reported that inhibiting the VEGF cascade altered the tumor microenvironment to the extent that nano DDSs were able to penetrate more easily.<sup>34</sup> They revealed that a VEGFR2 antibody DC101 increased pericyte coverage around the vasculature and decreased IFP. This reduction in IFP by inhibiting the VEGF cascade could also potentiate the distribution of LNPs in tumor tissue. Although the inhibition of the VEGF cascade can have both positive (regulating the tumor microenvironment, such as IFP) and negative impacts (vascular maturation) on the delivery of EPR-based nano DDSs, a positive impact caused by blocking VEGF signaling might be dominant in hypervascular cancer.

Besides, pericyte coverage and collagen degradation were increased in a siRNA-dose dependent manner (Figure 2c and Figure 3b). This dose-dependency suggests that altering tumor microenvironment would depend on an extent of VEGFR2 inhibition. Therefore, injections that are more frequent or an increase in the amount of siRNA would result in a more robust silencing of VEGFR2, and therefore more efficacious improvement in the distribution of large nanoparticles.

The suppression of VEGFR2 by si-VR2 evoked the infiltration of macrophages, and the subsequent ECMs degradation of MMPs by macrophages (Figure 4a,e). Thus, LNPs were able to deeply penetrate into tumor tissue. This infiltration can be attributed to the fact that the inhibition of VEGFR2 on endothelial cells forced them to produce some types of cytokines or chemokines that are attracted to monocytes in the blood stream. A previous report by Kroepper *et al.*, also suggested that inhibiting VEGFR2 by an antibody increased the levels of macrophages in a glioblastoma model, specifically M1-like phenotypes.<sup>35</sup> However, these investigators did not conclude that VEGFR2 was a factor in attracting M1 macrophages after treatment with a VEGFR2 antibody. The relationship between VEGF signaling and the tumor microenvironment including macrophages currently remain unclear. Further study will be needed to achieve an understanding of the involvement of macrophages on antiangiogenic therapy and our strategy.

However, macrophage infiltration is known to be an indicator of metastasis and a poor prognosis in patients.<sup>36</sup> Specifically M2 macrophages are immunosuppressive and support the proliferation of cancer cells, while M1 macrophages play a role in the antitumor effect by supporting immunoresponse.<sup>37</sup> We then determined the phenotypes of the induced macrophages by measuring M1 marker genes (inducible NO synthase (iNOS), Cxcl-9, IL-1 $\beta$ , IL-6, and TNF- $\alpha$ ) and M2 marker genes (mannose receptor C, Type 1 (MMR and Arginase-1) (see Supplementary Figure S11). In the case of M1 markers, Cxcl-9 and TNF- $\alpha$  were significantly increased while, in the case of M2 markers, MMR and Arginase-1 were decreased. This result suggests that macrophages induced by the injection of the RGD-MEND are M1-like macrophages. That is consistent with previous reports, in which the injection of an anti-VEGFR2 antibody DC101 evoked the production of M1-like macrophages, and consequently potentiated the efficacy

of immunoadjuvant therapy.<sup>38</sup> In addition, M1 macrophages supported an autoimmune system to exclude cancer cells.<sup>39</sup> Therefore, M1 macrophages elevation in our strategy would not induce a progress in infiltration and metastasis of cancer cells.

There is a possibility that siRNA was recognized by toll-like receptors 3, 7 or 8,<sup>40</sup> and thus macrophages were attracted by produced cytokines via immunostimulation of siRNA, not by VEGFR2 inhibition. We examined the immune reaction by the siRNA used in this study to exclude this possibility. To assess the immune response caused by the RGD-MEND encapsulating siRNA against VEGFR2 itself, we measured the presence of an interferon-induced protein with tetratricopeptide repeats 1, which was previously reported as a marker gene for an immune response to the presence of siRNA.<sup>41</sup> The findings indicated that interferon-induced protein with tetratricopeptide repeats 1 was not changed by the RGD-MEND injection (see Supplementary Figure S12) compared with the phosphate buffered saline (PBS) treatment. At this time, antipolo like kinase 1 siRNA (negative control), which was used as a nonimmunostimulatory siRNA as described in ref. 41, and not chemically modified si-VR2 (positive control) were also tested. As a result, the chemically modified si-VR2 used in this study failed to induce an immune response after its systemic injection. This result suggests that the immune response by the formulated siRNA did not contribute to the infiltration of macrophages, and that the inhibition of VEGFR2 itself induced the infiltration of macrophages.

ECMs are also known to be the factors in inhibiting the tumor penetration of nanoparticles, except for vasculature structures. Collagen degradation by the intratumoral injection of Type 1 collagenase was reported to increase the accumulation of liposomes in tumors.<sup>42</sup> Moreover, Frimpong *et al.*, studied the effect of the angiotensin receptor inhibitor, Losartan, on the penetration of intratumorally injected herpes simplex virus.<sup>43</sup> The Losartan treatment drastically improved the intratumoral penetration of herpes simplex virus, accompanied by the inhibition of TGF- $\beta$  production and subsequent decrease in Type 1 collagen levels. The same group also reported that this decrease in collagen content was the result of the deactivation of cancer-associated fibroblasts via the inhibition of the angiotensin II receptor-1.<sup>44</sup> These studies suggest that the stiffness of ECMs are important factors in the tumor penetration of nanoparticles, as opposed to vessel structure. Likewise, a si-VR2 treatment induced the degradation type 1 collagen due to the activation of MMPs (Figure 3a,d). The improved intratumoral distribution of LNPs could be caused by an increase in vascular dynamics through the infiltration of macrophages and the subsequent remodeling of vessels and/or ECMs. On the other hand, the production of high levels of MMPs is also known to facilitate metastasis via the degradation of the basement membrane around the vasculature.<sup>45</sup> If the basement membrane was degraded, cancer cell readily intravasate. Thus, MMPs production increased a risk for progression of cancer because intravasation is the first step of metastasis.<sup>46</sup> Based on these previous reports, the injection of the RGD-MEND might also promote metastasis from a primary tumor in our strategy. However, Type 4 collagen was not changed after the RGD-MEND treatment (see Supplementary Figure S9). This means that the increased MMPs are not likely involved in the degradation of the basement membrane, and consequently that

increased MMPs did not allow cancer cells to intravasate. Taken together, the improvement in intratumoral distribution through the inhibition of VEGFR2 by the RGD-MEND does not appear to be a risk factor for cancer metastasis. For developing this strategy, the effect of si-VR2 treatment on progression and/or metastasis should be investigated.

In this study, we show that the siRNA-mediated alteration in structural properties of the tumor vasculature and tumor micro-environment improved the distribution of LNPs, which results in a synergistic therapeutic effect when 100 nm DOX-LNP particles were used. As mentioned in the introduction section, small nanoparticles (<30 nm) have been found to easily extravasate and penetrate in tumor tissue deeply, whereas large nanoparticles (>100 nm) cannot.<sup>7</sup> This means that relatively large nanoparticles are not applicable for use in EPR-based nanotherapeutics. On the other hand, our findings suggest that regulating the tumor micro-environment via inhibiting VEGFR2 allows even large nanoparticles to extravasate and diffuse in tumor tissue. In short, the results show that relatively large nanoparticles (>100 nm) can be used in the above processes, thus expanding the spectrum of available nano DDSs.

The fact that the dynamics of the tumor vasculature and ECMs remodeling had a huge impact on the accumulation of LNPs raised some questions about the EPR effect-based strategy as a static phenomenon. It should, however, be noted that we have no perspective regarding with which types of cancers the improvement of nanoparticles could be induced by blockade in VEGF signaling. A previous study suggested that tumor vasculature phenotypes defined VEGF sensitivity.<sup>47</sup> In that study, stromal types (vasculature in stromal cells) was not responsive to anti-VEGF therapy, while the tumor type (vasculature in cancer cells) was sensitive. Likewise, the response to this strategy would depend on the type of cancer. Further study will clearly be required to elucidate the exact mechanism by which the anti-VEGF cascade-mediated improves the intratumoral distribution of nano DDSs. The control of the intratumoral distribution of nano DDSs by delivering siRNA to the tumor vasculature indicated that comparably large nanoparticles could deeply penetrate tumor tissue via controlling the tumor microenvironment, which represents an innovative approach for developing cancer-targeting nanotherapeutics.

## MATERIALS AND METHODS

**Materials.** Roswell Park Memorial Institute (RPMI) 1640, cholesterol and TriReagent were obtained from Sigma-Aldrich (St. Louis, MO). siRNA was synthesized by Hokkaido System Sciences (Sapporo, Japan). High-Capacity RNA-to-cDNA kit and Quanti-iT RiboGreen were purchased from ThermoFisher Scientific (Waltham, MA). THUNDERBIRD SYBR quantitative polymerase chain reaction (qPCR) Mix was purchased from TOYOBO (Osaka, Japan). Hoechst33342 was purchased from DOJINDO (Kumamoto, Japan). Chlondronate liposome was obtained from FormuMax (Palo Alto, CA). Polyethyleneglycol-dimyristoyl-glycerol (PEG-DMG), Polyethyleneglycol-distearoyl-glycerol (PEG-DSG) and distearoyl-sn-glycerophosphocholine (DSPC) were purchased from the NOF (Tokyo, Japan). Optimal Cutting Temperature (OCT) compound was obtained from Sakura Finetek Japan (Tokyo, Japan). Cyclic RGD was synthesized by Peptides international (Louisville, KY). Lipidic fluorescent dye 1,1'-dioctadecyl-3,3',3'-tetramethylindocarbocyanine perchlorate (DiI) and 1,1'-dioctadecyl-3,3',3'-tetramethylindocarbocyanine 4-chlorobenzenesulfonate salt (DiD) were purchased from PromoKine

(Heidelberg, Germany). The sequence of siRNA against VEGFR2 are as follows: Sense: cAaccAGAGAccuccGuaudTsdT, Antisense: AAACGAGGGUCUCUGGUUGdTsT (lower case; RNA, upper case; 2'-OMe, s; phosphorothioate linkage). Chemical modifications were carried out to reduce the immune response. Primers were synthesized by Sigma-Aldrich Japan (Ishikari, Japan). Primer sets used in this study were as follows: *Vegfr2*; forward GATTTTCACCTGGCACTCTCCTT, reverse GGTCACCTTGGTCAC *Mmp2*; forward TAAGCTCATCGCAGACTC, reverse *Mmp9*; forward CCCTCTGAATAAAGACGAC, reverse TATAGTGGGACACATAGTGG.

**In vivo experiment.** A human renal cell carcinoma cell line, OS-RC-2 cells were cultured in RPMI 1640 supplemented with 10% fetal bovine serum (FBS) and penicillin (100 U/ml), streptomycin (100 µg/ml) at 37°C under a 5% CO<sub>2</sub> humidified atmosphere. BALB/c nude mice were purchased from CLEA Japan (Shizuoka, Japan). To prepare tumor-bearing mice, euthymic mice were injected with 1 × 10<sup>6</sup> cells in 70 µl of PBS (-) on the right flank. All of the experiments with mice were performed when the tumor volume reached 100 mm<sup>3</sup>. The experimental protocols were approved by the Hokkaido University Animal Care Committee in accordance with the guidelines for the care and use of laboratory animals.

**LNPs preparation.** LNPs encapsulating siRNA was prepared by the tertiary butyl alcohol (*t*-BuOH) dilution method, as previously reported.<sup>13,48</sup> Lipids (3,000 nmol, YSK05/cholesterol/PEG-DMG, 70/30/3, molar ratio) in 400 µl of *t*-BuOH were gradually added to a siRNA solution, and the mixture was then added stepwise to 2.0 ml of citrate buffer (pH 4.0). The diluted mixture was rapidly added to 4.0 ml of PBS (-), and was then subjected to ultrafiltration by means of a Vivaspin (Sartorius Stedim Biotech, Goettingen, German: MWCO 100,000 Da) twice. This carrier has already been shown to accumulate in cancer cells, as previously reported.<sup>13</sup>

To target TECs, a cyclic RGD peptide conjugated to N-hydroxysuccinimide-PEG-distearoyl-*sn*-glycerolethanol amine (NHS-PEG2000-DSPE) (cRGD-PEG) was used. LNPs were modified with cRGD-PEG by incubating them for 30 minutes at 60°C in 7.5% of ethanol. After the incubation, the mixture was ultrafiltered by Vivaspin. Thus, the prepared RGD-MEND was able to deliver siRNA specifically to TECs.<sup>15</sup> When the LNPs were fluorescently labeled, a lipophilic dye, DiI or DiD was added to the lipid mixture prior to the first dilution. The recovery rate and encapsulation efficiency of siRNA were determined by RiboGreen. The LNPs were characterized with a ZetaSizer nano ZS (Malvern Instruments, Malvern, UK).

**Preparation of DOX-LPs.** Doxorubicin-loaded nanoparticles were prepared by a pH-loading method as previously reported.<sup>48</sup> Lipid thin films (4,000 nmol, DSPC/cholesterol/PEG-DSPE, 50/50/5, molar ratio) were prepared in glass tubes, and 500 µl of ammonium sulfate buffer (300 mmol/l, pH 4.5) was then added. The glass tubes were sonicated for 30 seconds in a bath-type sonicator (AU-25C, Aiwa, Tokyo, Japan) and then for 10 minutes with a probe-type sonicator (Misonix, Farmingdale, NY). The sonicated colloidal solution was then centrifuged (15,000×g, 10 minutes, room temperature) three times to remove debris at a sonication step. The supernatant was mixed with 200 µg of doxorubicin, and then incubated for 30 minutes at 60°C. Unloaded doxorubicin was removed by ultrafiltration with Vivaspin. The Doxorubicin content was determined by measuring the absorbance at 495 nm.

**FACS analysis for particle distribution.** To quantitatively assess the nanoparticle distribution in the tumor tissue, single dispersed tumor tissues were analyzed by flow cytometry. The collected tumor tissues were minced with scissors, and the resulting sample then incubated in a collagenase solution (2,800 U/ml of Type 1 collagenase, 100 µg/ml of DNase I, 5 mmol/l of CaCl<sub>2</sub>, 10% FBS in Hank's balanced salt solution) for 30 minutes at 37°C. Debris was then removed from the resulting suspension by passing it through a 100 µm cell strainer. To distinguish human cancer cells from other stromal cells, the cells were stained with an antihuman



HLA-A,B,C antibody (Biolegend, 311402) after blocking by a CD16/32 antibody (Biolegend, 101302). Cell was then assayed by flow cytometry (FACSCalibur, BD Biosciences, San Jose, CA). Propidium iodide positive cell populations were gated out as dead cells. The obtained data were analyzed with the CellQuest software

**Observation of LNPs distribution with raw tumor section.** To investigate the intratumoral distribution of LNPs, 400  $\mu\text{m}$  thick sections of tumor tissues were prepared using a Microslicer (DTK-1000, Dosaka-em, Kyoto, Japan) without being frozen. The sliced tumor sections was immersed in 10  $\mu\text{g}/\text{ml}$  Hoechst33342 and 10  $\mu\text{g}/\text{ml}$  Griffonia Simplicifolia isolectin B4 conjugated with FITC (Vector Laboratories, Burlingame, CA) or Alexa647 (ThermoFisher Scientific) observed by confocal laser scanning microscopy (A1, Nikon, Tokyo, Japan). To assess whether blood flows in the tumor vasculature, mice were systemically injected with 40  $\mu\text{g}$  of FITC-isolectin.

**Immunofluorescent analysis.** For immunostaining, paraformaldehyde-fixed tumor tissues were subjected to cryosection with CM3050S (Leica, Nussloch GmbH, German). Tumor sections were then immersed in the diluted antibody solutions (COL1A1 (NOVUS Biologicals, NB600-408), COLIV (Sigma-Aldrich, SAB4300738), F4/80 (Biolegend, 123101),  $\alpha\text{SMA}$  (Sigma-Aldrich, C6198), VEGFR2 (Biolegend, 136402)) for 1 hour. The sections were washed with PBS (-), and then treated with the appropriate secondary antibodies, and, finally, washed with PBS (-). The sections finally covered with cover glasses in the presence of VECTASHIELD Mounting Medium (Vector Laboratories, Peterborough, UK). The sections were then observed with A1 (Nikon).

**Hydroxyproline assay.** Hydroxyproline was analyzed as described in a previous report.<sup>49</sup> About 20 mg of tumor tissue was vigorously homogenized using 1.4 mm zirconium beads and hydro-lyzed for 5 hours at 120°C in an autoclave. The lysates were then centrifuged (15,000 $\times$ g, 10 minutes, 4°C), and 100  $\mu\text{l}$  aliquots of the supernatants were gently mixed with a 0.2 mol/l chloramine-T solution (acetate/citrate buffer (pH 6.5)/n-propanol. 90/10) for 2 hours at 4°C. Ehrlich's reagent (1 mol/l p-N,N-dimethylaminobenzaldehyde in n-propanol/60% perchloric acid 2/1) were added to the mixture, and then incubated for 30 minutes at 70°C. The solutions became clear yellow. Hydroxyproline contents were determined by measuring the absorbance of these solutions at 564 nm.

**Inhibition of MMPs and macrophages.** For inhibiting MMPs, a nonselective MMPs inhibitor, marimastat (MedChemExpress, Monmouth Junction, NJ), was administered 1 and 3 days before the collection at a dose of 30 mg/kg. To examine the effect of macrophages on nanoparticle distribution, liposomal clodronate (FormuMax) was intraperitoneally administered to tumor-bearing mice at a dose of 50 mg/kg.

**Quantitative reverse transcription-PCR analysis.** To assess the mRNA expression level, tumor tissues were minced with scissors, and preserved at -80°C until assayed. The minced tumor tissues were treated with 1.4 mm zirconium beads with PreCellys (Bertin Technologies, Montigny-le-Bretonneux, France) in 500  $\mu\text{l}$  of TriReagent. RNA extraction was done according to the manufacturer's instructions. cDNA was obtained by the reverse transcription of 1.0  $\mu\text{g}$  of total RNA with a RNA-to-cDNA kit using the following procedure: for 5 minutes at 60°C, denaturing for 10 minutes at 4°C, then for 60 minutes at 42°C, and finally for 5 minutes at 95°C for reverse transcription. The 50-times diluted cDNA was then subjected to quantitative reverse transcription-PCR with a THUNDERBIRD SYBR qPCR Mix. The mRNA expression levels were estimated by the  $\Delta\Delta\text{Ct}$  method.

## SUPPLEMENTARY MATERIAL

**Figure S1.** Characterization of LNPs.

**Figure S2.** VEGFR2 inhibition by RGD-MEND.

**Figure S3.** Change of intratumoral distribution of LNPs by single injection of RGD-MEND.

**Figure S4.** Methodology for evaluating OS-RC- 2 uptake of LNPs.

**Figure S5.** Change of the accumulation of LNPs by RGD-injection.

**Figure S6.** Effect of control siRNA formulated into RGD-MEND.

**Figure S7.** The effect of increasing the dose on intratumoral distribution.

**Figure S8.** Evaluation of collagen fibrils by Masson's trichrome staining.

**Figure S9.** The effect of formulated si-VR2 on type IV collagen.

**Figure S10.** Macrophage depletion by L-clodronate.

**Figure S11.** Determination of the phenotype of macrophages induced by the injection of RGD-MEND encapsulating si-VR2.

**Figure S12.** The immune response of the sequences of si-VR2 used in this study.

## ACKNOWLEDGMENTS

The authors thank Milton S Feather for modifying the manuscript. This study was supported partly by research grants (Research on Development of New Drugs, Health and Labour Sciences Research Grant, and Initiative for Accelerating Regulatory Science in Innovative Drug, Medical Device, and Regenerative Medicine) from the Japan Ministry of Health, Labour and Welfare (MHLW), Research Program on Hepatitis from Japanese Agency for Medical Research and development (AMED).

## AUTHOR CONTRIBUTIONS

Y.S. and H.H. designed all the experiments and wrote the manuscript. T.H. performed all the experiments. S.Y. assisted the flow cytometry analysis, and A.K. supported the experiments of macrophage depletion. W.M. supported *in vivo* experiments.

## ADDITIONAL INFORMATION

The authors declare no competing financial interests. Supplementary information Correspondence and requests for materials should be addressed to H.H.

## REFERENCES

- Maeda, H (2015). Toward a full understanding of the EPR effect in primary and metastatic tumors as well as issues related to its heterogeneity. *Adv Drug Deliv Rev* **91**: 3–6.
- Torchilin, V (2011). Tumor delivery of macromolecular drugs based on the EPR effect. *Adv Drug Deliv Rev* **63**: 131–135.
- Stapleton, S, Jaffray, D and Milosevic, M (2016). Radiation effects on the tumor microenvironment: Implications for nanomedicine delivery. *Adv Drug Deliv Rev* **16**: 30181–30188.
- Heldin, CH, Rubin, K, Pietras, K and Ostman, A (2004). High interstitial fluid pressure—an obstacle in cancer therapy. *Nat Rev Cancer* **4**: 806–813.
- Gong, H, Chao, Y, Xiang, J, Han, X, Song, G, Feng, L *et al.* (2016). Hyaluronidase to enhance nanoparticle-based photodynamic tumor therapy. *Nano Lett* **16**: 2512–2521.
- McKee, TD, Grandi, P, Mok, W, Alexandrakis, G, Insin, N, Zimmer, JP *et al.* (2006). Degradation of fibrillar collagen in a human melanoma xenograft improves the efficacy of an oncolytic herpes simplex virus vector. *Cancer Res* **66**: 2509–2513.
- Cabral, H, Matsumoto, Y, Mizuno, K, Chen, Q, Murakami, M, Kimura, M *et al.* (2011). Accumulation of sub-100 nm polymeric micelles in poorly permeable tumours depends on size. *Nat Nanotechnol* **6**: 815–823.
- Ishida, T and Kiwada, H (2013). Alteration of tumor microenvironment for improved delivery and intratumor distribution of nanocarriers. *Biol Pharm Bull* **36**: 692–697.
- Danhier, F and Préat, V (2015). Strategies to improve the EPR effect for the delivery of anti-cancer nanomedicines. *Cancer Cell & Microenvironment* **2**: e808.
- Parekh, H and Rini, BI (2015). Emerging therapeutic approaches in renal cell carcinoma. *Expert Rev Anticancer Ther* **15**: 1305–1314.
- Hada, T, Sakurai, Y and Harashima, H (2015). Optimization of a siRNA carrier modified with a pH-sensitive cationic lipid and a cyclic RGD peptide for efficiently targeting tumor endothelial cells. *Pharmaceutics* **7**: 320–333.
- Yamamoto, N, Sato, Y, Munakata, T, Kakuni, M, Tateo, C, Sanada, T *et al.* (2016). Novel pH-sensitive multifunctional envelope-type nanodevice for siRNA-based treatments for chronic HBV infection. *J Hepatol* **64**: 547–555.
- Sakurai, Y, Hatakeyama, H, Sato, Y, Hyodo, M, Akita, H and Harashima, H (2013). Gene silencing via RNAi and siRNA quantification in tumor tissue using MEND, a liposomal siRNA delivery system. *Mol Ther* **21**: 1195–1203.
- Liu, S (2006). Radiolabeled multimeric cyclic RGD peptides as integrin alphavbeta3 targeted radiotracers for tumor imaging. *Mol Pharm* **3**: 472–487.
- Sakurai, Y, Hatakeyama, H, Sato, Y, Hyodo, M, Akita, H, Ohga, N *et al.* (2014). RNAi-mediated gene knockdown and anti-angiogenic therapy of RCCs using a cyclic RGD-modified liposomal-siRNA system. *J Control Release* **173**: 110–118.
- Robinson, CM and Ohh, M (2014). The multifaceted von Hippel-Lindau tumour suppressor protein. *FEBS Lett* **588**: 2704–2711.
- Matsuda, K, Ohga, N, Hida, Y, Muraki, C, Tsuchiya, K, Kurosu, T *et al.* (2010). Isolated tumor endothelial cells maintain specific character during long-term culture. *Biochem Biophys Res Commun* **394**: 947–954.

18. Watanabe, T, Hatakeyama, H, Matsuda-Yasui, C, Sato, Y, Sudoh, M, Takagi, A *et al.* (2014). *In vivo* therapeutic potential of Dicer-hunting siRNAs targeting infectious hepatitis C virus. *Sci Rep* **4**: 4750.
19. Goel, S, Duda, DG, Xu, L, Munn, LL, Boucher, Y, Fukumura, D *et al.* (2011). Normalization of the vasculature for treatment of cancer and other diseases. *Physiol Rev* **91**: 1071–1121.
20. Neuman, RE and Logan, MA (1950). The determination of collagen and elastin in tissues. *J Biol Chem* **186**: 549–556.
21. Vandenbroucke, RE and Libert, C (2014). Is there new hope for therapeutic matrix metalloproteinase inhibition? *Nat Rev Drug Discov* **13**: 904–927.
22. Coussens, LM, Tinkle, CL, Hanahan, D and Werb, Z (2000). MMP-9 supplied by bone marrow-derived cells contributes to skin carcinogenesis. *Cell* **103**: 481–490.
23. Cortez-Retamozo, V, Etzrodt, M, Newton, A, Rauch, PJ, Chudnovskiy, A, Berger, C *et al.* (2012). Origins of tumor-associated macrophages and neutrophils. *Proc Natl Acad Sci USA* **109**: 2491–2496.
24. Hashizume, H, Baluk, P, Morikawa, S, McLean, JW, Thurston, G, Roberge, S *et al.* (2000). Openings between defective endothelial cells explain tumor vessel leakiness. *Am J Pathol* **156**: 1363–1380.
25. Maeda, H (2010). Nitroglycerin enhances vascular blood flow and drug delivery in hypoxic tumor tissues: analogy between angina pectoris and solid tumors and enhancement of the EPR effect. *J Control Release* **142**: 296–298.
26. Wu, J, Akaike, T and Maeda, H (1998). Modulation of enhanced vascular permeability in tumors by a bradykinin antagonist, a cyclooxygenase inhibitor, and a nitric oxide scavenger. *Cancer Res* **58**: 159–165.
27. Fontanella, C, Ongaro, E, Bolzonello, S, Guardascione, M, Fasola, G and Aprile, G (2014). Clinical advances in the development of novel VEGFR2 inhibitors. *Ann Transl Med* **2**: 123.
28. Vennepureddy, A, Singh, P, Rastogi, R, Atallah, JP and Terjanian, T (2016). Evolution of ramucirumab in the treatment of cancer - A review of literature. *J Oncol Pharm Pract* (epub ahead of print).
29. Park, S, Kim, JW, Kim, JH, Lim, CW and Kim, B (2015). Differential roles of angiogenesis in the induction of fibrogenesis and the resolution of fibrosis in liver. *Biol Pharm Bull* **38**: 980–985.
30. DeLeve, LD (2015). Liver sinusoidal endothelial cells in hepatic fibrosis. *Hepatology* **61**: 1740–1746.
31. Lin, SL, Chang, FC, Schrimpf, C, Chen, YT, Wu, CF, Wu, VC *et al.* (2011). Targeting endothelium-pericyte cross talk by inhibiting VEGF receptor signaling attenuates kidney microvascular rarefaction and fibrosis. *Am J Pathol* **178**: 911–923.
32. Iredale, JP, Benyon, RC, Pickering, J, McCullen, M, Northrop, M, Pawley, S *et al.* (1998). Mechanisms of spontaneous resolution of rat liver fibrosis. Hepatic stellate cell apoptosis and reduced hepatic expression of metalloproteinase inhibitors. *J Clin Invest* **102**: 538–549.
33. Siemens, DR, Heaton, JP, Adams, MA, Kawakami, J and Graham, CH (2009). Phase II study of nitric oxide donor for men with increasing prostate-specific antigen level after surgery or radiotherapy for prostate cancer. *Urology* **74**: 878–883.
34. Tong, RT, Boucher, Y, Kozin, SV, Winkler, F, Hicklin, DJ and Jain, RK (2004). Vascular normalization by vascular endothelial growth factor receptor 2 blockade induces a pressure gradient across the vasculature and improves drug penetration in tumors. *Cancer Res* **64**: 3731–3736.
35. Kloepper, J, Riedemann, L, Amoozgar, Z, Seano, G, Susek, K, Yu, V *et al.* (2016). Ang-2/VEGF bispecific antibody reprograms macrophages and resident microglia to anti-tumor phenotype and prolongs glioblastoma survival. *Proc Natl Acad Sci USA* **113**: 4476–4481.
36. Biswas, SK, Allavena, P and Mantovani, A (2013). Tumor-associated macrophages: functional diversity, clinical significance, and open questions. *Semin Immunopathol* **35**: 585–600.
37. Komohara, Y, Fujiwara, Y, Ohnishi, K and Takeya, M (2016). Tumor-associated macrophages: Potential therapeutic targets for anticancer therapy. *Adv Drug Deliv Rev* **99**(Pt B): 180–185.
38. Huang, Y, Yuan, J, Righi, E, Kamoun, WS, Ancukiewicz, M, Nezivar, J *et al.* (2012). Vascular normalizing doses of antiangiogenic treatment reprogram the immunosuppressive tumor microenvironment and enhance immunotherapy. *Proc Natl Acad Sci USA* **109**: 17561–17566.
39. Italiani, P and Boraschi, D (2014). From monocytes to M1/M2 macrophages: Phenotypical vs. functional differentiation. *Front Immunol* **5**: 514.
40. Robbins, M, Judge, A and MacLachlan, I (2009). siRNA and innate immunity. *Oligonucleotides* **19**: 89–102.
41. Judge, AD, Robbins, M, Tavakoli, I, Levi, J, Hu, L, Fronza, A *et al.* (2009). Confirming the RNAi-mediated mechanism of action of siRNA-based cancer therapeutics in mice. *J Clin Invest* **119**: 661–673.
42. Zheng, X, Goins, BA, Cameron, IL, Santoyo, C, Bao, A, Frohlich, VC *et al.* (2011). Ultrasound-guided intratumoral administration of collagenase-2 improved liposome drug accumulation in solid tumor xenografts. *Cancer Chemother Pharmacol* **67**: 173–182.
43. Diop-Frimpong, B, Chauhan, VP, Krane, S, Boucher, Y and Jain, RK (2011). Losartan inhibits collagen I synthesis and improves the distribution and efficacy of nanotherapeutics in tumors. *Proc Natl Acad Sci USA* **108**: 2909–2914.
44. Chauhan, VP, Martin, JD, Liu, H, Lacombe, DA, Jain, SR, Kozin, SV *et al.* (2013). Angiotensin inhibition enhances drug delivery and potentiates chemotherapy by decompressing tumour blood vessels. *Nat Commun* **4**: 2516.
45. Mittal, R, Patel, AP, Debs, LH, Nguyen, D, Patel, K, Grati, M, *et al.* (2016). Intricate functions of matrix metalloproteinases in physiological and pathological conditions. *J Cell Physiol* **231**: 2599–2621.
46. Blazejczyk, A, Papiernik, D, Porshneva, K, Sadowska, J and Wietrzyk, J (2015). Endothelium and cancer metastasis: Perspectives for antimetastatic therapy. *Pharmacol Rep* **67**: 711–718.
47. Smith, NR, Baker, D, Farren, M, Pommier, A, Swann, R, Wang, X *et al.* (2014). Tumor stromal phenotypes define VEGF sensitivity–response. *Clin Cancer Res* **20**: 5141.
48. Sakurai, Y, Hatakeyama, H, Akita, H and Harashima, H (2014). Improvement of doxorubicin efficacy using liposomal anti-polo-like kinase 1 siRNA in human renal cell carcinomas. *Mol Pharm* **11**: 2713–2719.
49. Reddy, GK and Enwemeka, CS (1996). A simplified method for the analysis of hydroxyproline in biological tissues. *Clin Biochem* **29**: 225–229.